Microfluid Nanofluid (2014) 17:527–537
DOI 10.1007/s10404-014-1336-8

RESEARCH PAPER

Understanding drop-pattern formation in 2-D microchannels: a multi-agent approach

M. Danny Raj · R. Rengaswamy

Received: 31 August 2013 / Accepted: 4 January 2014 / Published online: 24 January 2014

Abstract We propose a modeling strategy to simulate drop movement in a two-phase flow inside a 2-D diverging–converging microchannel. These are planar channels that allow 2-D movement of drops. The increasing cross-sectional area of the diverging section decelerates the drop, and the decreasing cross-sectional area of the converging section accelerates it. These drops as they slow down approach each other and start to interact hydrodynamically and form 2-D arrangements inside the microchannel. We propose interacting drop-traffic models, that are phenomenological in nature, to characterize the different interactions of a drop with the neighboring drops, continuous phase and the channel walls. By incorporating these models into a multi-agent simulation, that employs Newton's second law of motion along with the creeping flow approximation, we are able to predict the positions and velocities of all the drops inside the microchannel. The time evolution of the dynamic 2-D patterns formed by the drops inside the microchannel is investigated. We are able to qualitatively understand the features in a microchannel that aid the formation of the 2-D patterns. The simulation strategy helps us to understand the layering phenomena that results in the formation of the 2-D structures near the diverging section and the breaking patterns of drops near the converging section of the microchannel.

Keywords Phenomenological models · Drop movement · Multi-agent approach · Diverging–converging microchannels

1 Introduction

The drop-continuous two-phase flow in a microchannel offers a lot of advantages. One can compartmentalize the fluid of interest as a drop (Huebner et al. 2008; Kelly et al. 2007; Song et al. 2006), achieve convective apart from diffusive mixing inside the drop (Bringer et al. 2004; Kelley 2008) and design devices where there is very little wastage of fluid of interest by wetting. Also, these drops can be manipulated and processed inside the channel, subject to different conditions according to the need (Maddala et al. 2012; Niu et al. 2007, 2009). For design of systems that employ drops, there is a need for mathematical models to explain the movement of these drops inside the microchannel. This is typically a fluid mechanics problem which can be solved using the Navier–Stokes equation along with the continuity equation in both the phases (Gupta et al. 2009; Jovanović et al. 2011; Taha and Cui 2006). But the high computational costs of these CFD simulations restrict their use in optimization and design, encouraging simple models for drop movement in microchannels.

Simple models have been used to investigate 1-D microchannels, notably the microfluidic loops (Jousse et al. 2005) where the authors propose a network model to understand drop movement in the microchannels. Later simple models were used to understand flow of drops in simple and dual microfluidic networks and to study the nonlinear and complex behavior of simple microfluidic loops (Schindler and Ajdari 2008; Sessoms et al. 2009) as

Electronic supplementary material The online version of this article (doi:10.1007/s10404-014-1336-8) contains supplementary material, which is available to authorized users.

M. Danny Raj · R. Rengaswamy (✉)
Department of Chemical Engineering, Indian Institute of Technology Madras, 150, Mechanical Sciences Block, Chennai 600036, India
e-mail: raghur@iitm.ac.in

seen in experiments (Fuerstman et al. 2007). The simplicity of these models allowed its incorporation into a model predictive control routine to study active manipulation of drops inside the channel (Maddala et al. 2012).

In 2-D microchannels, like in the Hele-Shaw flow-geometry, the drops are sandwiched between the upper and lower boundaries but not constrained by the side walls, which allow free movement in the available 2-D space. Drops interact and self-organize to form patterns in these microchannels (Jose and Cubaud 2012; Thorsen et al. 2001) and also show dynamic clustering behavior (Beatus et al. 2009). This self-assembly is of interest to polymer technology where complex micro-particles are made by thermal fusing (Sung et al. 2008) and to emulsion science (Chu et al. 2007; Hashimoto et al. 2007). Beatus and coworkers have studied many body physics of drops in 1-D and 2-D configurations. They consider a dipole-like hydrodynamic interaction between drops and were able to explain some interesting non-equilibrium phenomena (Beatus et al. 2006, 2012). This work was followed up by Uspal and Doyle (2012), extended by Desreumaux et al. (2013) and applied to an ensemble of drops. Effect of drop deformation on the collective dynamics was studied by Janssen et al. (2012). The very low Reynolds number associated with the flow result in the linear creeping flow equations that describe the flow field in the microchannel. Particle motion in the flow field in the Lagrangian description can be expressed by $\dot{\vec{x}} = v(\vec{x})$ where v is non-linear in space. Instances when the motions of the particles becoming chaotic have been investigated (Aref 1983; Jones et al. 1989). In our case, nonlinearity arises due to two reasons. First is the nonlinear velocity field of the continuous phase that will result in the motion of the drops inside the microchannel, and the second reason is due to coupling of the motion between the drop and the continuous phase. There is lubrication flow between the drops when they come close to each other. High-pressure fields are generated that prevent the approach of the drops. One will have to resolve the time and spatial scales to capture this multi-scale effect. This encourages the development of simpler simulation strategies to investigate these systems. The focus of this article is to introduce a simple modeling framework to visualize drop movement in 2-D micro-channels. We restrict our analysis to those microchannels that are symmetric about their longitudinal axis.

2 System of interest

The *microchannel system* chosen for validation is a linearly diverging–converging microchannel, symmetric about the horizontal axis (Fig. 1). The dimensions of the microchannel were kept the same as in the experiments (Jose and Cubaud 2012) ($k = 0.5$; $W = 4.75$ mm; $H = 5$ mm). When the drops enter the channel at a very small rate, a single layer of drops are formed inside the microchannel. As the rate of entry of drops increase, the drops acquire a multilayer conformation. The entry frequency is manipulated in the experiments by controlling the input velocity of drops and the initial spacing between them. However, in the experiments (Jose and Cubaud 2012), these two manipulated variables were correlated as $L_0/2R = 0.45(Q_{continuous}/Q_{drop})$ where L_0 is the initial spacing between the drops, R is the radius and Q is the flow rate, because of the dynamics of the drop generator. For the purpose of validation, we used the same correlation in our simulations.

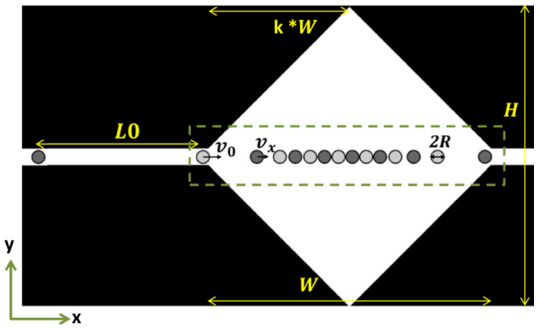

Fig. 1 Microchannel system chosen for validation of simulation results. Geometry same as (Jose and Cubaud 2012) *dotted part* in the microchannel is where the drop arrangement is seen; $k = 0.5$; $W = 4.75$ mm; $H = 5$ mm; $R = 0.125$ mm

For the simulation, all the geometrical parameters k, W, H and operating parameters v_0, R, L_0 (Fig. 1) are kept the same as the experiments of Jose and Cubaud (2012) and the patterns formed are compared.

3 Modeling strategy

3.1 Multi-agent framework (MAS)

Multi-agent models are a class of models used to investigate collective behavior of a group of interacting agents. These agents follow simple rules for interacting with themselves and the surroundings and result in complex behavior. This approach has found applications in biology to study the flocking of birds, fish schools, swarm modeling, etc. (Reynolds 1987), in economics and finance to model the human interactions (Bonabeau 2002), in traffic to simulate vehicle dynamics (Naiem et al. 2010) and in many other areas.

The *Multi-agent* approach looks at drops as agents inside the microchannel system. These drops (agents) follow certain rules for interaction with other drops and the surroundings. A similar approach has been used to study complex behavior of drops in microfluidic loop

devices (Smith and Gaver 2010). If one is able to characterize the different forces acting on each drop, then it is possible to determine its position and velocity by solving the Newton's second law of motion as shown in Eq. (1), for all the drops simultaneously. The drops do not undergo any significant deformation which allows us to assume a circular shape. Hence, it is sufficient to track the centers of these circular drops. Also, the 2-D nature of the flow results in the center of masses of all the drops to lie on the x–y plane.

$$M_i \frac{d\vec{U}_i}{dt} = \sum \vec{F}_i \tag{1}$$

The very low Reynolds number ($N_{\mathrm{Re}} < 1$) of the system allows us to use the creeping flow approximation according to which the inertial contribution of the system becomes negligible simplifying Eq. (1) to give Eq. (2).

$$\sum \vec{F}_i = 0 \tag{2}$$

3.2 Interacting drop-traffic models

Interacting drop-traffic models provide a simple description for the different forces acting on the drop inside the microchannel. Three principle forces that act on the drop are considered. The *force due to the flow of the continuous phase* is a result of the pressure driven flow that forces the drop to move. The converging–diverging microchannels we are interested in are symmetric about the horizontal axis and so is the flow of the continuous phase. The total resistance to the flow is influenced by the y position of the drops in the microchannel. Let us consider the case where there is only one drop in the microchannel. The configuration where the drop is at the line of symmetry results in the least resistance for flow, which can be determined by calculating the pressure drop as a function of the y position of the drop. When the drop is at this position, the average velocities on either side of the drop in the y direction (above and below the drop) are the same because of the symmetry.

Inspired by the solution to the classic problem of stokes flow past a sphere, the x-component of the force is assumed to be proportional to the relative velocity between the drop and the continuous phase (Leal 2007). The first term of the RHS of Eq. (3) explains the relative velocity between the drop and the local average of the continuous phase velocity. One can also look at the x-component force as a superposition of the forcing due to the flow of the continuous phase $k_f\left(\langle v_{a,i}\rangle + \langle v_{b,i}\rangle/2\right)$ and the drag on the drop due to its movement in the viscous continuous phase $-(K_f\beta\, U_{i,x}$. The y-component force on the drop will be such that a drop will move in a way that will reduce the difference in the velocities above and below the drop, locally ensuring

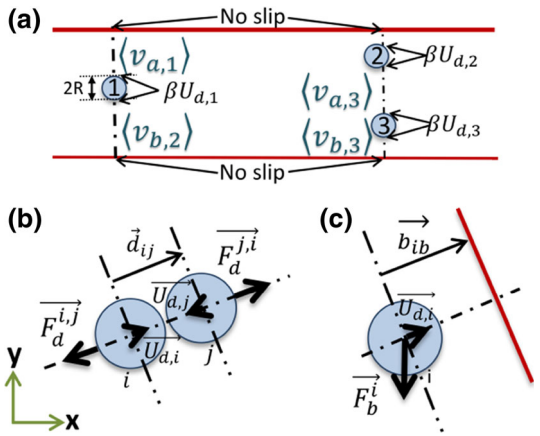

Fig. 2 **a** Boundary conditions to estimate the approximate flow patterns around the drop; $\langle v_{a,i}\rangle$ is the average velocity above drop i and similarly $\langle v_{b,i}\rangle$ for average velocity below the drop. **b** Force between drops due to lubrication flow of continuous phase between the drops; the force is along the line joining the centers of the two drops. **c** Force on the drop as it approaches the boundary (wall), due to the lubrication flow of continuous phase between the drop and boundary; Force is along the line joining the center to the closest point in the channel boundary

least resistance for flow around the drop. Hence, it takes the form $k_f k'\left(\langle v_{a,i}\rangle - \langle v_{b,i}\rangle\right)$. The force on the drop due to its motion in the viscous continuous phase is $-K_f\beta\, U_{i,y}$. The superposition of the two results in $k_f\left(k'\left(\langle v_{a,i}\rangle - \langle v_{b,i}\rangle\right) - \beta\, U_{i,y}\right)$ as explained by the second term in Eq. (3). If $\langle v_{a,i}\rangle$ and $\langle v_{b,i}\rangle$ are the average velocities of continuous phase above and below drop 'i' which has a velocity $\vec{U}_i = U_{i,x}\hat{e}_x + U_{i,y}\hat{e}_y$, then the force due to flow of continuous phase $\vec{F}_{f,i}$ is characterized by Eq. (3) where β is the ratio of the velocity of continuous phase at the drop interface to the translational velocity of the drop.

$$\begin{aligned}\vec{F}_{f,i} = {} & k_f\left(\frac{\langle v_{a,i}\rangle + \langle v_{b,i}\rangle}{2} - \beta U_{i,x}\right)\hat{e}_x \\ & + k_f\left(k'\left(\langle v_{a,i}\rangle - \langle v_{b,i}\rangle\right) - \beta U_{i,y}\right)\hat{e}_y\end{aligned} \tag{3}$$

Knowledge of the approximate velocity profiles of the continuous phase fluid above and below the drop $v_{a,i}$ and $v_{b,i}$, respectively, is now essential to estimate the average velocities. Similar to the solution to the pressure driven flow through infinite parallel plates, we assume a parabolic flow profile above and below the drop as shown in Eq. (4) [chapter 3 (Leal 2007)].

$$\begin{aligned} v_{a,i} &= A_i y^2 + B_{i,a} y + C_{i,a} \\ v_{b,i} &= A_i y^2 + B_{i,b} y + C_{i,b} \end{aligned} \tag{4}$$

When only one drop is present in the microchannel at a given area of cross section, $v_{a,i}$ represents the velocity profile of the continuous phase bounded by the top wall and drop boundary and $v_{b,i}$ represents the velocity profile

bounded by the drop boundary and the bottom wall (see drop 1 in Fig. 2a). If there is a drop above the selected drop as illustrated in Fig. 2a (see drop 3), then $v_{a,i}$ represents the velocity profile of continuous phase bounded by drop 2 and drop 3 and $v_{b,i}$ represents the velocity profile bounded by the drop boundary and the bottom wall. This can be extended similarly for the case where there are drops on either side of drop 'i'. The constants in Eq. (4) can be calculated using the information available about the flow in the problem such as the no-slip condition at the walls of the microchannel $v_{a,i} = 0$, continuity of velocities at the drop interface $v_{a,i} = \beta U_i$ as shown in Fig. 2a and the mass conservation which is applied to the cross section of the microchannel containing the center of mass of the drop 'i'. The term A_i in Eq. (4) is kept the same for a given cross section because it approximately characterizes the pressure gradient due to the resistance offered for the flow. One should note that A_i is minimal when the drop is at the center, in the single-drop case.

If we consider the motion of a single drop along the center of the microchannel, the only force acting on the drop would be the x-component of the force due to the flow of the continuous phase F_f which results in drop velocity as explained by Eq. (5).

$$U_{i,x} = \frac{1}{\beta}\left(\frac{\left(\langle v_{a,i}\rangle + \langle v_{b,i}\rangle\right)}{2}\right) \tag{5}$$

Experimentally, it has been observed by Jose and Cubaud (2012) that the velocity of the drop is proportional to the superficial velocity of the fluid in the 1-D geometry. In the network model, this information is explicitly used while calculating the velocity of the drops (Schindler and Ajdari 2008; Smith and Gaver 2010). Sessoms et al. (2009) considered the effects of pressure drop on the continuous phase and drop phase separately and were able to estimate the velocity of the drop as a multiple of the superficial velocity. In the drop-traffic models, we consider internal circulations inside the drop, by stating that the velocity of the continuous phase at the drop–fluid interface is βU_d. In Eq. (5), $\langle v_{a,i}\rangle$ and $\langle v_{b,i}\rangle$ are functions of U_i. With boundary conditions and mass conservation, it is possible to express the constants in Eq. (4) analytically to get an expression for the velocity of the drop U_i. On simplification, we get Eq. (6) where d represents the depth in the direction perpendicular to the 2-D flow area and H represents the width of the channel in the y direction (perpendicular to the longitudinal direction).

$$U_{i,x} = \frac{Q_{total}}{d \times (2R(1-\beta) + \beta \times H)} \tag{6}$$

In a 2-D microchannel, the large cross section, presence of other drops and the complex flow fields complicate the determination of β associated with the drop.

The drops experience a *force* $\vec{F}_d^{i,j}$ *that resists their relative motion when they come close to each other* as shown in Fig. 2b. This is explained by lubrication theory for the asymptotic case of drops approaching each other (Davis et al. 1989). The functional form of the force is given in Eq. (7), which explains the force between drops in the microchannel where $\vec{d}_{i,j}$ is the vector from drop 'i' to drop 'j'. k_d and γ are tuning parameters. The force is unbounded because of the denominator term in Eq. (7) which ensures that the drops never touch each other. The interaction force considered is different from that used by Beatus and coworkers, which considers a dipole-like hydrodynamic interaction between drops (Beatus et al. 2006). Because coalescence dynamics is not considered, attractive forces are not taken into account.

$$\vec{F}_d^{i,j} = \begin{cases} \left(\frac{k_d \dot{d}_{i,j}}{\left\|\vec{d}_{i,j}\right\| - 2R}\right)\hat{d}_{j,i} & \left\|\vec{d}_{i,j}\right\| > \gamma R, \dot{d}_{i,j} > 0 \\ 0 & else \end{cases} \tag{7}$$

where,

$$\dot{d}_{i,j} = \vec{U}_i.\hat{d}_{i,j} + \vec{U}_j.\hat{d}_{j,i}$$

Force due to the converging boundary $\vec{F}_b^{i,b}$ is computed by an expression as shown in Eq. (8) where α_1, α_2 and k_b are tuning parameters. The asymptotic problem of sphere moving toward a wall (Leal 2007) has a functional form as in Eq. (8) which is similar to Eq. (7), where $\vec{b}_{i,b}$ is the vector connecting the drop, to the closest point on the boundary. However, only the y-component of this force is considered when the drop is farther away from the boundary, and along with F_f, this explains the motion of the drop in the converging section of the channel as shown in Fig. 2c.

$$\vec{F}_b^{i,b} = \begin{cases} \left(\frac{k_b \dot{b}_{i,b}}{\left\|\vec{b}_{i,j}\right\| - R}\right)\hat{b}_{b,i} & \left\|\vec{b}_{i,b}\right\| \le \alpha_1 R, \dot{b}_{i,b} > 0 \\ \left(\frac{k_b \dot{b}_{i,b}\left(\hat{b}_{b,i}.\hat{e}_y\right)}{\left\|\vec{b}_{i,j}\right\| - R}\right)\hat{e}_y & \alpha_1 R < \left\|\vec{b}_{i,b}\right\| \le \alpha_2 R, \dot{b}_{i,b} > 0 \\ 0 & else \end{cases}$$

where,

$$\dot{b}_{i,b} = \vec{U}_i.\hat{b}_{i,b}; a_1 < a_2 \tag{8}$$

This functional form ensures that the drop stays inside the microchannel. Drops flowing parallel to the wall experience no force due to the wall because the rate at which they approach it $\dot{b}_{i,b}$ goes to zero. Because the drops experience a force only when they are very close to each other or the wall, the effect of these forces is neglected when they are farther than γR and $\alpha_2 R$ from the neighboring drop and boundary, respectively.

3.3 Algorithm for simulating drop movement

In this section, we present a stepwise algorithm to implement the MAS with the interacting drop-traffic models to simulate drop movement inside a microchannel.

Step 1 Guess *x*- and *y*- component of velocities of all n drops. (A good guess would be to use the superficial velocities of the continuous phase)

Step 2.1 Go to the position of drop *i* where $i \in \{1,2,\ldots,n\}$ and identify the number of drops in that area of cross section of the microchannel. Let this number be m.

[Note: number of drops can be identified by solving the line that represents the projection of the area of cross section in 2-D space (*x*–*y*) with the equation of the circle (center: position of each drop, radius: *R*).]

Step 2.2 Find the average continuous phase velocities $\langle v_{a,i} \rangle$ and $\langle v_{b,i} \rangle$ above and below each of the m drops. To do so, one needs to estimate 2 m + 3 parameters according to Eq. (4).

Step 2.3 Uniquely determine the parameters by using the 2m conditions that arise out of the continuity of velocity across each drop, two no-slip conditions and one mass conservation equation across the cross-sectional area.

[Note: to find the force on drop '*i*' due to the flow, it is required to estimate the average velocities above and below the drop '*i*'. But to do so, we would have to use the mass conservation condition to estimate the constants. This needs the information of the flow in the entire area of cross section. This is why in step 2.3, we calculate the velocities above and below all the drops in a given area of cross section.]

Step 2.4 Repeat steps 2.1–2.3 to find the average velocities above and below all the drops in the microchannel.

Step 2.5 Estimate $\vec{F}_{f,i}$ and $\vec{F}_d^{i,j}$ for all the drops using Eqs. (3) and (7), respectively.

Step 3.1 Estimate the point in the boundary closest to drop i and estimate $\vec{b}_{i,b}$.

Step 3.2 Calculate $\vec{F}_b^{i,b}$ using Eq. (8) for every drop.

Step 4 Compute the total force on each drop $\sum \vec{F}_i$.

Step 5 Check if Eq. (2) is satisfied. If not, update the guess and repeat steps 2–4. If satisfied, go to step 6.

Step 6 Update the positions of the drops in the microchannel and go back to step 1.

It is possible to generate a movie from the simulation result by plotting the positions of the drops at each instant of time and capturing the image as a frame. All the frames can be combined into a movie, which serves as a better visual aid in analyzing drop movement inside the microchannel. This was done using MATLAB's *Videowriter*. [See supplementary information for movie results.]

Table 1 Tuned parameters

k_f	$6\pi\mu R$
k_d	$3 \times 6\pi\mu R^2$
k_b	$10 \times 6\pi\mu R^2$
γ	$2.4R$
β	1
α_1	$2.4R$
α_2	10
k'	1/4

4 Tuning

Because the models are not derived from first principles and are approximate, the functional forms for the forces on the drop contain tuning parameters k_f, k_d, k_b, α_1, α_2, β, γ that have to be tuned to match the experiments. From Eq. (2), because the sum of the forces is zero, one can infer that the ratios of the *k*'s are important and not the absolute values. The values used for the simulation are listed in Table 1. Tuning was performed to make sure that the simulation was able to predict the different layered configurations for approximately similar operating conditions as in the experiments (Jose and Cubaud 2012). The uncertainty in the correlations provided by Jose and Cubaud (2012) that relate the operating conditions (ref Sect. 2), made the comparison of the experimental data with the simulation results tedious. No rigorous algorithm was followed to tune the models. Constants that accompanied the solution to the asymptotic cases as explained in Sect. 3.2 are retained and the integers multiplying these constants were manipulated to tune the model. Tuning was done based on the visual perception. The ease of tuning indicates the robustness of the simulation strategy to changes in the tuning parameters. One should note that once the tuning parameters are set, only the operating parameters are varied to identify the different structures formed inside the microchannel.

5 Dynamic pattern formation

5.1 One-layer configuration

The drops entering the microchannel decelerate in the diverging section and accelerate in the converging section due to the increasing and decreasing cross-sectional area for flow. The distances between the drops decrease as they

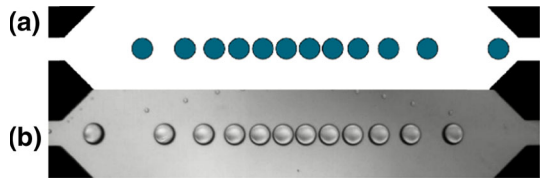

Fig. 3 (Enhanced online) One-layer configuration: **a** multi-agent simulation (>500 ms) ($L_0 = 38R$); **b** experiments ($L_0 \approx 30R$) (Jose and Cubaud 2012)[Enhanced online]

slow down and increase as they speed up in the microchannel. As the inlet spacing is reduced, the distance between the drops in the microchannel reduces and they start to interact hydrodynamically as explained by Eq. (7). For an inlet spacing as large as $L_0 = 38R$ prior to the entry into the microchannel, a single layer of drops is formed as shown in Fig. 3. One should realize that all the forces, the force on the drop due to the flow (F_f) and the hydrodynamic drop–drop interactions (F_d), are constrained to the x direction for the one-layer arrangement of drops. Absence of a y-component of force would mean that the drops can never escape the single-layer conformation. To capture the effect of the y-component forces, the walls of the microchannel are modified with a practically infinitesimal random roughness factor. This results in a nonzero y-component of F_f [Eq. (3)] which continuously perturbs the drops from their one-layer arrangement, mimicking reality where disturbances are ubiquitous. As the drops start to interact, the y-component of the force F_d, between the drops as explained by Eq. (7), tries to push the drops to the next layer while the y-component of the F_f tries to preserve the one-layer configuration. We observed that a competition between the drop–drop interaction forces and the y-component of the force due to flow decided the stability of the one-layer arrangement. For a given inlet spacing, the simulation was carried out for different random roughness in the wall. We observed that all the simulations were identical.

5.2 Two-layer configuration: the phenomenon of layering

When the initial spacing between the drops is reduced further ($L_0 < 35R$), drops start to crowd in the diverging section of the channel. The small disturbance present in the system grows in time because of the drop–drop interactions, resulting in the displacement of a drop from the one-layer arrangement. Because the drop–drop interactions are directed along the line joining the centers of two drops, the displaced drop upsets its neighbors, and this process continues resulting in a chain reaction that propagates backward in the microchannel (see Fig. 4a), offsetting the drops from their initial arrangement, causing layering. The drops

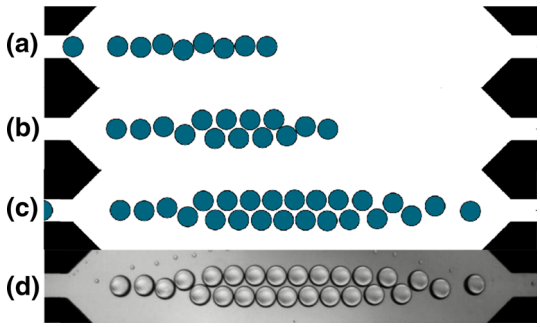

Fig. 4 (Enhanced online) Two-layer configuration: multi-agent simulation ($L_0 = 18R$): **a** 140 ms, **b** 240 ms, **c** >500 ms; *d* Experiments ($L_0 = 14R$) (Jose and Cubaud 2012) [Enhanced online]

as they come in arrange themselves in two layers (see Fig. 4b). In the converging section of the channel, the accelerating velocity field pulls the drops from the layered structure to form a single layer before exiting the channel (see converging section in Fig. 4c), because the size of the exit channel is of the same order of magnitude of the size of the drop ($2R$). Layering observed in the system under consideration is similar to the zigzag instability, observed by Beatus and coworkers. They observe this instability near the drop formation area and attribute it to the asymmetry in the microfluidic crystal (drop near the channel entrance perturbed from the axis of symmetry) (Beatus et al. 2006). In our simulations, the asymmetry in the system stems from the roughness factor added to the channel walls that result in the perturbation of drops in the transverse direction.

5.3 Three-layer configuration

For even lower initial spacing of drops ($L_0 < 16R$), the single layer of drops initially formed become unstable (Fig. 5a) as explained in the previous section and the drops temporarily assume a two-layer arrangement (Fig. 5b). Unable to house the entering drops, the two-layer arrangement eventually becomes unstable (Fig. 5c) and the system drifts away to the next configuration where there are three layers of drops (Fig. 5d, e). The breaking of the two-layer arrangement is similar to that of the one-layer arrangement where the drop that moves away from the layered structure perturbs all of its neighbor drops destabilizing both the layers. In the converging section of the channel, the drop structure breaks down in a complex manner to form a single layer of drops before exit. The multi-agent simulation was able to capture these fine qualitative details seen in the experimental videos like the zigzag nature of the middle layer of drops in the three-layer conformation (Fig. 5e, f). For even smaller inlet spacing ($L_0 < 11R$), multiple layers (>3) are observed.

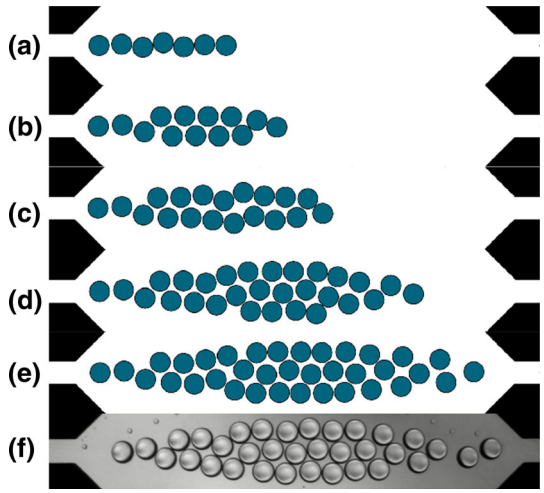

Fig. 5 (Enhanced online) Three-layer configuration: multi-agent simulation ($L_0 = 12R$): **a** 75 ms, **b** 140 ms, **c** 207 ms, **d** 320 ms, **e** >500 ms; *f* experiments ($L_0 = 12R$) (Jose and Cubaud 2012) [Enhanced online]

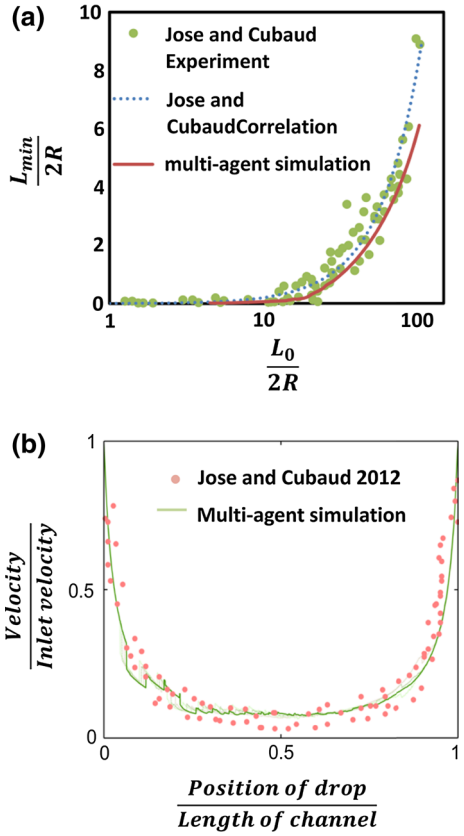

Fig. 6 **a** The minimum distance between two drops inside a microchannel as a function of the inlet spacing: comparison between the experimental results and empirical correlation (Jose and Cubaud 2012) with the multi-agent simulation; **b** velocity of drops as a function of its position in the channel: comparison between the experimental results (Jose and Cubaud 2012) with the multi-agent simulations. [Experimental data were digitized from Jose and Cubaud 2012]

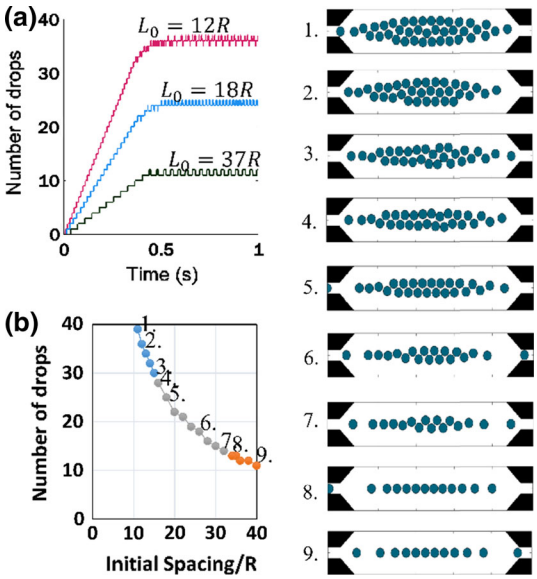

Fig. 7 **a** Time evolution of the number of drops in the microchannel for initial spacing that give one, two and three layers; **b** a plot of the number of drops inside a microchannel as a function of the initial spacing between the drops prior to entry into the channel, along with the snapshots of the patterns formed by the drops

5.4 Quantitative characterization

When the minimum distance between drops at a particular fixed inlet feeding frequency in the microchannel is evaluated, it is found to be in good agreement with the experimental results (Fig. 6a). A comparison of the velocities of the drops inside the microchannel with the experimental results is showed in Fig. 6b. The multi-agent simulation was able to predict the trend in the velocity profiles which was similar to the superficial velocity profiles for the channel geometry as experimentally observed by Jose and Cubaud (2012). The fluctuations in the velocity profiles can be attributed to the piecewise nature of the functional forms Eqs. (7) and (8).

As the drops enter the microchannel, they start to form a dynamic structure. The number of drops inside the microchannel increases steadily till the drop front reaches the exit of the diverging–converging microchannel. The number of drops inside the channel stabilizes, and a steady dynamic structure is formed (Fig. 7a). This is because the rate at which the drops exit is equal to the rate at which they enter. As the initial spacing is reduced, larger structures are formed and so the number of drops inside the channel also increases (Fig. 7b).

6 Reasons for pattern formation

The multi-agent simulation helps us to understand the connection between the rich patterns formed by the drops

and the geometry of the microchannel. One of the important insights is, even with the drop–drop interactions, the velocity of the drops lies in the neighborhood of the superficial velocities (Fig. 6b). This fact helps us to understand pattern formation qualitatively. One might be interested in understanding the features of the microchannel that resulted in the rich patterns. From Fig. 6b, it is clear that we can approximate the velocity field inside the microchannel as a combination of linear decrease in velocity with length at the entrance, flat low velocity midregion and a linear increase in velocity near the exit. The deceleration field near the diverging entrance and low velocity in a large part of the midsection are the two important features of the microchannel under study (rectangular) that we believe affects the pattern formation. To address this issue, we investigate the dynamics of drops in four different channels. All the four microchannels considered have the same minimum and maximum width of the channel (in the y direction) as that of the rectangular channel. This ensured that the inlet and the minimum superficial velocities were identical. The initial spacings between drops that were used to compare the dynamics were the same as the ones that gave one ($L_0 = 37R$), two ($L_0 = 18R$) and three ($L_0 = 12R$) layer configurations for the rectangular microchannel.

First we consider *Microchannel-1*, with superficial velocity fields, linearly decreasing and increasing along the length (Fig. 8a). From Fig. 8c, e, g, one can observe that the drops did not layer as expected. Now the next question would be to find out the features of the microchannel that will result in pattern formation. This encouraged us to design *Microchannel-2* in which the length of the diverging section is increased (Fig. 8b, d, f, h). We can observe from Fig. 8d, f, h that the drops layered as expected and could form one and two layers and two layers becoming unstable. In comparison with the Microchannel-1, the rate at which the superficial velocity decreased along the length of Microchannel-2 is lower. This feature of the microchannel aids in the formation of layered arrangements. Deceleration of drops in microchannel-2 is lower than 1 but the time spent by drops in the diverging section is higher in 2 than in 1. Because the drop feeding rate is kept constant for both the microchannels, the number of drops in the diverging section of microchannel-2 is greater than that of 1. This results in more crowding of drops and aids in the formation of layered configurations.

Microchannel-3 is designed to understand the effect of the low flat velocity midsection in the microchannel (Fig. 8i). From Fig. 8k, m and o, it is clear that the patterns formed are close to one, two and three layers. This is the result of the similarity between microchannel-3 and the rectangular microchannel because the velocity profile of 3 (Fig. 8i) captures features of the velocity profile of the rectangular microchannel (Fig. 6b). Dynamics of drops in microchannel-2 helps us to understand the role of a slowly diverging section of a microchannel in pattern formation. Hence, *microchannel-4* was designed with an intent to understand the combined effect of the slow deceleration and flat velocity sections of the microchannel (Fig. 8j). From Fig. 8l, n and p, one can conclude that the qualitative features of the patterns formed are the same as microchannel-3. The increased number of drops and close packing of drops in the patterns formed in microchannel-4 are due to the excessive crowding of drops in the slow-diverging sections. It becomes clear from the above analysis that the low flat velocity midsection of the microchannel has a greater effect on pattern formation than the diverging section of the microchannel. This is the reason for the rich patterns observed by Jose and Cubaud (2012) in their rectangular geometry.

7 Future work

The interacting drop-traffic models discussed in Sect. 3.2 give very simple descriptions for the forces experienced by a drop inside a microchannel. Improving the model would make the MAS more general to 2-D microchannels. Also, the tuning parameters in the models are functions of system properties like the viscosities and densities of the liquids and their interfacial tension and geometry. Understanding these relations through another set of models would make the simulation technique ready for use in optimization. One should note that the MAS framework is such that it provides room for improvement. Based on the observations of the experiments (Jose and Cubaud 2012), phenomenological models were developed for explaining drop dynamics in 2-D channels. When new physics concerning drop flow in 2-D microchannel is observed, its contribution to the force balance can be added to Eq. (2). This way it is possible to incorporate the effect of any new phenomena in the MAS and to study their impact on pattern formation. As Reynolds number increases inertial effects start to dominate. To study the system, it is enough to relax the creeping flow assumption and solve the complete Newton's second law of motion as given in Eq. (1). Another interesting observation was the propagated coalescence in microchannels crowded with drops, reported by Bremond and coworkers (Bremond et al. 2008). They believe that it might be a possible route to achieve phase inversion of the two immiscible phases. It is an interesting problem because when two immiscible liquids flow in a microchannel, the liquid that wets the wall most becomes the continuous phase and the other liquid becomes the discrete drop phase. A phase inversion event is not surfactant driven unlike macro-systems (Shui et al. 2009). But in a 2-D

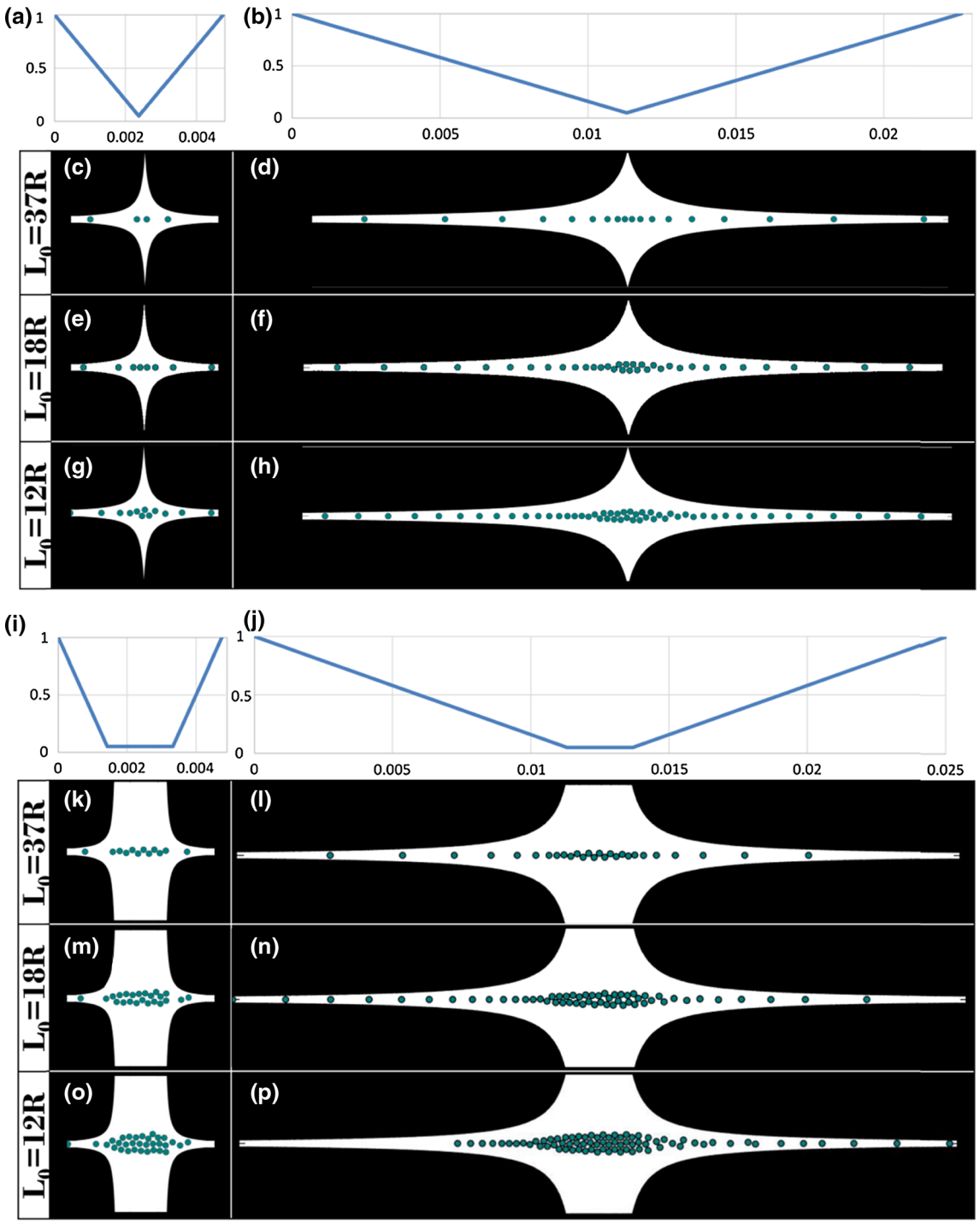

Fig. 8 **a** Velocity profile of microchannel-1 (**c**, **e**, **g**); **b** velocity profiles of microchannel-2 (**d**, **f**, **h**); **c**–**h** Microchannels with superficial velocities linearly decreasing in the diverging section and linearly increasing in the converging section; **i** velocity profile of microchannel-3 (**k**, **m**, **o**); **j** velocity profiles of microchannel-4 (**l**, **n**, **p**); **k**–**p** Microchannels with linearly decreasing superficial velocity in the diverging section followed by a region of constant velocity followed by a linearly increasing superficial velocity in the converging section [Enhanced online]

microchannel, is may be possible through a set of coalescence events. The first step toward predicting this phenomenon computationally would be to understand drop arrangement inside a 2-D microchannel, which has been addressed in the present article. The next obvious step would be to understand drop coalescence modes through a

set of models and to incorporate them with the MAS to study the propagated coalescence as a function of geometry and predict phase inversion.

8 Conclusions

We propose a simulation strategy to predict the dynamic pattern formation of drops in a 2-D diverging–converging microchannel. We proposed simple intuitive models for the significant forces experienced by the drops inside the microchannel through the interacting drop-traffic models. Incorporation of these models into a multi-agent simulation that solved the Newton's second law of motion helped in simulating the dynamics of these drop arrangements. The multi-agent simulation aided in the investigation of the phenomenon of layering in the diverging section of the channel which gave rise to the layered configuration, and the breaking patterns in the converging section of the channel just before the exit. The simulation helped us understand the relation between geometry and patterns formed inside the microchannel. Features of the microchannel that aided in the pattern formation were studied by constructing suitable microchannels that decoupled the effect of the individual features. We were able to understand why the rectangular geometry of Jose and Cubaud (2012) was able to produce such rich patterns. The phenomenological nature of the models results in tuning parameters that need to be adjusted. These parameters are functions of the system properties like the viscosities and densities of both the fluids and the interfacial tension. The fact that new phenomena can be added to the interacting drop-traffic models makes the MAS approach a versatile technique to understand drop dynamics in 2-D microchannels. We believe that this is the first step toward the development of a powerful computational tool for drop-microfluidic research.

Acknowledgments We would like to thank the reviewers for their comments and pointing to relevant literature that improved the quality of the paper. We would like to thank Jason R Picardo and other members of the Pushpavanam research league in IIT Madras, India, for the dynamic and helpful discussions. We would also like to thank Bibin M. Jose and Thomas Cubaud (Stony Brook University, USA) for sharing their experimental video of drops moving inside the microchannel which was not available in the literature.

References

Aref H (1983) Stirring by chaotic advection. J Fluid Mech 143:1–21. doi:10.1017/S0022112084001233

Beatus T, Tlusty T, Bar-Ziv R (2006) Phonons in a one-dimensional microfluidic crystal. Nat Phys 2:743–748. doi:10.1038/nphys432

Beatus T, Tlusty T, Bar-Ziv R (2009) Burgers shock waves and sound in a 2D microfluidic droplets ensemble. Phys Rev Lett 103:114502. doi:10.1103/PhysRevLett.103.114502

Beatus T, Bar-Ziv RH, Tlusty T (2012) The physics of 2D microfluidic droplet ensembles. Phys Rep 516:103–145. doi:10.1016/j.physrep.2012.02.003

Bonabeau E (2002) Agent-based modeling: methods and techniques for simulating human systems. Proc Natl Acad Sci USA 99(Suppl 3):7280–7287. doi:10.1073/pnas.082080899

Bremond N, Thiam A, Bibette J (2008) Decompressing emulsion droplets favors coalescence. Phys Rev Lett 100:1–4. doi:10.1103/PhysRevLett.100.024501

Bringer MR, Gerdts CJ, Song H et al (2004) Microfluidic systems for chemical kinetics that rely on chaotic mixing in droplets. Philos Trans A Math Phys Eng Sci 362:1087–1104. doi:10.1098/rsta 2003.1364

Chu L-Y, Utada AS, Shah RK et al (2007) Controllable monodisperse multiple emulsions. Angew Chem Int Ed Engl 46:8970–8974. doi:10.1002/anie.200701358

Davis RH, Schonberg JA, Rallison JM (1989) The lubrication force between two viscous drops. Phys Fluids A Fluid Dyn 1:77. doi:10.1063/1.857525

Desreumaux N, Caussin J-B, Jeanneret R et al (2013) Hydrodynamic fluctuations in confined particle-laden fluids. Phys Rev Lett 111:118301. doi:10.1103/PhysRevLett.111.118301

Fuerstman MJ, Garstecki P, Whitesides GM (2007) Coding/decoding and reversibility of droplet trains in microfluidic networks. Science 315:828–832. doi:10.1126/science.1134514

Gupta R, Fletcher DF, Haynes BS (2009) On the CFD modelling of Taylor flow in microchannels. Chem Eng Sci 64:2941–2950. doi:10.1016/j.ces.2009.03.018

Hashimoto M, Garstecki P, Whitesides GM (2007) Synthesis of composite emulsions and complex foams with the use of microfluidic flow-focusing devices. Small 3:1792–1802. doi:10.1002/smll.200700238

Huebner A, Sharma S, Srisa-Art M et al (2008) Microdroplets: a sea of applications? Lab Chip 8:1244–1254. doi:10.1039/b806405a

Janssen PJA, Baron MD, Anderson PD et al. (2012) Collective dynamics of confined rigid spheres and deformable drops †. 7495–7506. doi:10.1039/c2sm25812a

Jones SW, Aref H, Thomas OM (1989) Chaotic advection by laminar flow in a twisted pipe. J Fluid Mech 209:335–357

Jose BM, Cubaud T (2012) Droplet arrangement and coalescence in diverging/converging microchannels. Microfluid Nanofluidics 12:687–696. doi:10.1007/s10404-011-0909-z

Jousse F, Lian G, Janes R, Melrose J (2005) Compact model for multi-phase liquid–liquid flows in micro-fluidic devices. Lab Chip 5:646–656. doi:10.1039/b416666c

Jovanović J, Zhou W, Rebrov EV et al (2011) Liquid–liquid slug flow: hydrodynamics and pressure drop. Chem Eng Sci 66:42–54. doi:10.1016/j.ces.2010.09.040

Kelley KW (2008) Reactions in droplets in microfluidic channels. Brain Behav Immun 22:629. doi:10.1016/j.bbi.2008.05.010

Kelly BT, Baret J-C, Taly V, Griffiths AD (2007) Miniaturizing chemistry and biology in microdroplets. Chem Commun (Camb) 1773–88. doi:10.1039/b616252e

Leal LG (2007) Advanced transport phenomena. doi:10.1017/CBO9780511800245

Maddala J, Srinivasan B, Bithi SS et al (2012) Design of a model-based feedback controller for active sorting and synchronization of droplets in a microfluidic loop. AIChE J 58:2120–2130. doi:10.1002/aic.12740

Naiem A, Reda M, El-Beltagy M, El-Khodary I (2010) An agent based approach for modeling traffic flow. Informatics Syst (INFOS), 7th Int Conf 1:28–30

Niu X, Zhang M, Peng S et al (2007) Real-time detection, control, and sorting of microfluidic droplets. Biomicrofluidics 1:044101

Niu X, Zhang M, Wu J et al (2009) Generation and manipulation of "smart" droplets. Soft Matter 5:576. doi:10.1039/b816553j

Reynolds CW (1987) Flocks, herds and schools: a distributed behavioral model. ACM SIGGRAPH Comput Graph 21:25–34. doi:10.1145/37402.37406

Schindler M, Ajdari A (2008) Droplet traffic in microfluidic networks: a simple model for understanding and designing. Phys Rev Lett. doi:10.1103/PhysRevLett.100.044501

Sessoms D, Belloul M, Engl W et al (2009) Droplet motion in microfluidic networks: hydrodynamic interactions and pressure-drop measurements. Phys Rev E 80:1–10. doi:10.1103/PhysRevE.80.016317

Shui L, van den Berg A, Eijkel JCT (2009) Interfacial tension controlled W/O and O/W 2-phase flows in microchannel. Lab Chip 9:795–801. doi:10.1039/b813724b

Smith BJ, Gaver DP (2010) Agent-based simulations of complex droplet pattern formation in a two-branch microfluidic network. Lab Chip 10:303–312. doi:10.1039/b916380h

Song H, Chen DL, Ismagilov RF (2006) Reactions in droplets in microfluidic channels. Angew Chem Int Ed Engl 45:7336–7356. doi:10.1002/anie.200601554

Sung KE, Vanapalli SA, Mukhija D et al. (2008) Programmable fluidic production of microparticles with configurable anisotropy. 1335–1340

Taha T, Cui ZF (2006) CFD modelling of slug flow inside square capillaries. Chem Eng Sci 61:665–675. doi:10.1016/j.ces.2005.07.023

Thorsen T, Roberts RW, Arnold FH, Quake SR (2001) Dynamic pattern formation in a vesicle-generating microfluidic device. Phys Rev Lett 86:4163–4166. doi:10.1103/PhysRevLett.86.4163

Uspal WE, Doyle PS (2012) Collective dynamics of small clusters of particles flowing in a quasi-two-dimensional microchannel. Soft Matter 8:10676. doi:10.1039/c2sm25931a